doi: 10.4149/gpb_2026025

Icariin alleviates abdominal aortic aneurysm by targeting CYP1B1 to inhibit M1 polarization and VSMC apoptosis

Xiaosen Liu[1], Shuzhen Li[1], Jian Wang[1] and Zexiang Tian[1]

[1] *Department of Cardiothoracic Surgery, The Affiliated Hospital of Inner Mongolia Medical University, Hohhot, Inner Mongolia, China*

Abstract. Abdominal aortic aneurysm (AAA) is a life-threatening vascular disease with limited medical therapies. The role and targets of icariin, a flavonoid from Epimedium brevicornu Maxim, in AAA remain unclear. First, transcriptomic data from the GEO dataset GSE183464 were analyzed to screen differentially expressed genes (DEGs). DEGs were then integrated with M1 polarization-related genes (GeneCards) and icariin-targeted genes (CTD/SwissTargetPrediction) using Venn analysis, and the obtained candidate genes were subjected to GO and KEGG enrichment analyses. Machine learning (LASSO and Random Forest) was employed to prioritize core targets from a gene expression matrix, followed by molecular docking (AutoDock Vina) for assessing the binding affinity between icariin and Cytochrome P450 Family 1 Subfamily B Member 1 (CYP1B1), and visualizing (PyMOL and Discovery Studio) the binding modes. The effects of icariin were evaluated in THP-1-derived macrophages. Bioinformatics identified 15 candidate genes; machine learning converged on CYP1B1/BCL2L11. Molecular docking confirmed icariin's high affinity for CYP1B1. Icariin dose-dependently inhibited LPS/IFN-γ-induced M1 polarization and NF-κB activation, while CYP1B1 overexpression reversed these effects. Icariin also reduced M1-induced VSMC apoptosis. By demonstrating that icariin alleviates AAA by targeting CYP1B1 to suppress NF-κB-driven M1 polarization and VSMC apoptosis, this study establishes the icariin-CYP1B1 axis as a promising therapeutic strategy.

Key words: Abdominal aortic aneurysm — Icariin — CYP1B1 — M1 macrophage polarization — NF-κB — Vascular smooth muscle cell apoptosis

Introduction

Abdominal aortic aneurysm (AAA) constitutes a life-threatening vascular disorder, distinguished primarily by the progressive expansion of the abdominal aorta (Haque et al. 2022; Wang et al. 2023). Despite a growing understanding of AAA pathophysiology, effective medical therapies remain elusive, making surgical intervention the mainstay treatment to prevent rupture in eligible cases, highlighting an urgent need for novel targets (Cho et al. 2023; Puertas-Umbert et al. 2023). To understand why therapeutic options remain limited, it is critical to first examine AAA's core pathogenesis: chronic inflammation, extracellular matrix degradation, and vascular smooth muscle cell (VSMC) apoptosis, driven primarily by M1 macrophage polarization and aberrant NF-κB activation (Shioi et al. 2018; Chang et al. 2020; Lu et al. 2021). Activated M1 macrophages secrete proinflammatory cytokines (e.g., TNF-α and IL-6) and matrix metalloprotein-

Electronic supplementary material. The online version of this article (10.4149/gpb_2026025) contains Supplementary material.
Correspondence to: Zexiang Tian, Department of Cardiothoracic Surgery, the Affiliated Hospital of Inner Mongolia Medical University, No. 1, Tongdao North Street, Huimin District, Hohhot, Inner Mongolia, China
E-mail: tianzexiang_1985@126.com

ases, disrupting aortic structure, while NF-κB mediates both M1 polarization and VSMC apoptosis (Huang et al. 2024; Xu et al. 2025). However, the specific molecules linking these processes remain poorly defined, hindering targeted therapy development.

Against this backdrop, natural products like icariin, a major flavonoid from Epimedium brevicornu Maxim, have emerged as promising cardiovascular therapeutics (Sánchez-Gutiérrez et al. 2024). Icariin suppresses macrophage foam cell formation in atherosclerosis and mitigates myocardial ischemia-reperfusion injury (Fang et al. 2017). However, its potential effects on M1 polarization and VSMC survival in the context of AAA, as well as the specific targets involved, have not been investigated. A potential candidate target is Cytochrome P450 Family 1 Subfamily B Member 1 (CYP1B1), a CYP450 enzyme linked to vascular inflammation: CYP1B1 deficiency reduces macrophage cytokine production and ameliorates vascular remodeling in hypertension, yet its expression and function in AAA and interaction with icariin are unknown (Du et al. 2025). To bridge these gaps, integrative bioinformatics and machine learning have become indispensable tools for target discovery in complex diseases, enabling systematic screening of transcriptomic data and prioritization of candidate genes (Zhou et al. 2024). Machine learning techniques, as a key application of artificial intelligence (AI) in advancing medical research and target identification (Ahuja et al. 2024; Ogbonna et al. 2025), were employed to prioritize core targets from the gene expression matrix, enhancing the reliability of our candidate gene selection. Such approaches can accelerate the identification of molecules connecting inflammation, VSMC dysfunction, and AAA, addressing the limitations of traditional experimental methods.

To systematically elucidate the molecular targets and mechanisms underlying icariin's potential therapeutic effects on AAA, an integrated approach combining computational screening with experimental validation was implemented. First, a systematic screening *via* bioinformatics and machine learning was conducted to pinpoint core targets; subsequently, the interaction between icariin and the prioritized target was structurally validated; finally, the functional role of this target in mediating icariin's effects on M1 polarization and its consequential impact on VSMC apoptosis was mechanistically elucidated. This work aims to provide a novel molecular basis for icariin's therapeutic potential against AAA.

Materials and Methods

Bioinformatics analysis

Transcriptomic data of AAA tissues were retrieved from the Gene Expression Omnibus (GEO) database under the accession number GSE183464, which includes RNA sequencing data from 14 human abdominal aortic tissue samples (7 AAA patients and 7 healthy controls). Raw data were normalized using the limma R package, and differentially expressed genes (DEGs) between the AAA and control groups were identified with the thresholds of adj. $p < 0.05$ and $|\log_2(\text{fold change, logFC})| > 2$. A volcano plot was generated *via* GraphPad Prism to visualize DEGs.

Meanwhile, genes implicated in M1 macrophage polarization were compiled from the GeneCards database (https://www.genecards.org/) by applying a filter for a Relevance Score greater than 10 to the search term M1 macrophage polarization, thereby ensuring a high degree of functional association. Additionally, potential targets of icariin were predicted by interrogating both the Comparative Toxicogenomics Database (CTD, https://ctdbase.org/) and the SwissTargetPrediction platform (https://www.swisstargetprediction.ch/). A non-redundant gene set representing icariin targets was then created through the combination of findings derived from these two separate databases, along with the elimination of duplicate entries.

The three gene sets (AAA DEGs, M1 polarization-related genes, and icariin-targeted genes) were uploaded to the Venny online tool (https://bioinfogp.cnb.csic.es/tools/venny/) for intersection analysis. The overlapping genes were defined as icariin-AAA potential target genes. Their expression profiles from the GSE183464 dataset were visualized in a heatmap using the pheatmap package in R. The heatmap included hierarchical clustering of both samples (comparing AAA versus control) and genes.

To further characterize the biological functions and pathways associated with these DEGs, Gene Ontology (GO) functional enrichment analysis (including biological process (BP), cellular component (CC), and molecular function (MF)) and Kyoto Encyclopedia of Genes and Genomes (KEGG) pathway enrichment analysis were performed using the clusterProfiler R package. Enrichment terms were considered statistically significant at an adjusted p-value < 0.05. The top 10 significantly enriched terms for each category were visualized using bubble plots.

Least absolute shrinkage and selection operator (LASSO) regression

First, a gene expression matrix (15 potential genes × 14 samples) from GSE183464 was constructed, with sample groups (AAA = 1, control = 0) as the response variable. The penalty parameter λ was optimized *via* 10-fold cross-validation, and the λ value corresponding to the minimum partial likelihood deviance (λ.min) was selected to minimize overfitting. Genes with non-zero coefficients under λ.min were considered LASSO-screened targets. A coefficient path plot and a partial likelihood deviance plot were generated to illustrate the gene selection process.

Random forest (RF)

The randomForest package was used to build an RF classifier. The same gene expression matrix and response variable as LASSO were used, with the count of decision trees (denoted as ntree) fixed at 500, and the number of variables sampled per split (referred to as mtry) optimized through cross-validation. The importance of each potential gene was evaluated by the Mean Decrease in Gini index, which reflects the contribution of a gene to sample classification accuracy. Genes with an importance score in the top 50% were defined as RF-screened targets, and a feature importance bar plot was generated. The targets screened by LASSO and RF were uploaded to Venny 2.1 for intersection analysis. Genes shared by both algorithms were identified as core target genes for subsequent validation.

Molecular docking

Both the ligand (icariin) and the protein target (human CYP1B1, PDB ID: 3PM0) were prepared for docking using AutoDock Vina. The structure of icariin was acquired from the PubChem database, after which Gasteiger charges were added, and nonpolar hydrogen atoms were merged. The protein structure was obtained from the PDB, followed by the removal of water molecules and co-crystallized ligands using PyMOL 2.5 and modeling of missing side chains using the Swiss-Model server. Finally, both molecules were converted to PDBQT format within AutoDock Tools, with Kollman united atom charges added to the protein.

The binding pocket of CYP1B1 was defined based on its active site, with a grid box set to 20×20×20 Å (x: 50.0, y: 45.0, and z: 38.0) and a grid spacing of 0.375 Å. For comparison, BCL2L11 (another core target, PDB ID: 2BZW) was processed using the same protocol and docked with icariin. The docking run was performed with exhaustiveness set to 32, and the binding energy (kcal/mol) of the most stable conformation was recorded. A binding energy more negative than −5 kcal/mol was considered indicative of strong binding affinity. The most stable icariin-CYP1B1 docking complex was visualized using PyMOL 2.5 to show intermolecular interactions (hydrogen bonds, π-alkyl interactions, and van der Waals forces). A 2D interaction diagram was generated using Discovery Studio Visualizer 21.1 to label residue-specific contacts between icariin and CYP1B1.

Cell lines and culture conditions

The human monocytic leukemia THP-1 cell line (ScienCell, San Diego, CA, USA) was maintained in RPMI 1640 medium (Gibco, Grand Island, NY, USA) supplemented with 2 mM L-glutamine, 4.5 g/l glucose, 10 mM HEPES, 1.0 mM sodium pyruvate, 10% heat-inactivated fetal bovine serum (FBS, Gibco), and 1% antibiotic-antimycotic mixture (Gibco). Primary human abdominal aortic VSMCs (ScienCell) were grown in Smooth Muscle Cell Medium (ScienCell) containing 5% FBS, 1% smooth muscle cell growth supplement (Invitrogen, Carlsbad, CA, USA), and 1% antibiotic-antimycotic mixture. Both cell types were incubated under standard conditions at 37°C in a humidified atmosphere of 5% CO_2. The growth medium was refreshed at 2–3 day intervals to keep THP-1 cells within a density range of 5×10^4 to 8×10^5 cells/ml. To ensure phenotypic stability, the VSMCs were utilized between passages three and five.

Cell differentiation and polarization

THP-1 monocytes were first plated in 6-well plates at a density of 2×10^6 cells *per* well, and subsequently exposed to 100 nM phorbol 12-myristate 13-acetate (PMA; Sigma-Aldrich, St. Louis, MO, USA) for a 24 h incubation. After differentiation, the medium was discarded, and cells were washed twice with phosphate-buffered saline (PBS, Gibco) to remove residual PMA.

For M1 macrophage polarization, differentiated macrophages were assigned to the following groups: a control group receiving no stimulation; an LPS/IFN-γ group treated with 100 ng/ml LPS and 50 ng/ml IFN-γ; two intervention groups receiving LPS/IFN-γ along with either 5 μM or 10 μM icariin; a rescue group transfected with CYP1B1 overexpression plasmid and treated with LPS/IFN-γ and icariin; and an independent CYP1B1 overexpression group (and its corresponding empty vector control group) that was transfected with plasmid/vector but received no icariin pretreatment and no LPS/IFN-γ stimulation. Cells were pre-incubated with icariin (at least 98% pure) for 1 h before being stimulated with LPS/IFN-γ for 24 h. Cells in the independent overexpression groups were cultured in complete medium for 24 h under identical conditions, without any additional treatment. Icariin was dissolved in DMSO (Sigma-Aldrich), with a final concentration of less than 0.1%, which was confirmed to be non-cytotoxic.

Cell transfection and co-culture

The CYP1B1 overexpression plasmid (pcDNA3.1-CYP1B1, hereinafter and in the figures referred to as "CYP1B1") and the empty vector (pcDNA3.1) were obtained from a commercial source (GenScript, Nanjing, China). THP-1 macrophages were transfected with 2 μg plasmid/vector using Lipofectamine 3000 (Invitrogen, Carlsbad, CA, USA) following the manufacturer's protocol. Indirect co-culture was conducted using a Transwell system (pore diameter of 0.4 μm, Corning, Corning, NY, USA). Specifically, THP-1 macrophages were plated in the upper compartment at a density of 1×10^6 cells *per* insert, while VSMCs were seeded in the lower compartment at 1×10^6 cells *per* well in a 6-well

plate. Co-cultures were maintained in RPMI 1640 medium with 1% FBS for 24 h, after which VSMCs were collected for apoptosis-related protein detection.

Cell counting kit-8 (CCK-8) assay

Cell viability was assessed using the CCK-8 (Beyotime Biotechnology, Shanghai, China) according to the manufacturer's instructions. Briefly, THP-1-derived macrophages were placed in 96-well plates at 1×10^4 cells *per* well. After cells were treated with 1-50 μM icariin for 24 h, 10 μl of CCK-8 solution was added to each well and incubated at 37°C for 2 h. A microplate reader (BioTek Instruments, Winooski, VT, USA) was employed to measure the absorbance at 450 nm.

Western blotting (WB)

Cells were washed twice with PBS and lysed in RIPA buffer (Beyotime Biotechnology) supplemented with 1% protease inhibitor cocktail (Beyotime Biotechnology) and 1% phosphatase inhibitor cocktail (Beyotime Biotechnology) on ice for 30 min. Lysates were centrifuged at 12000×*g* for 15 min at 4°C, and supernatants (total protein) were collected. Protein concentration was measured using a BCA protein assay kit (Beyotime Biotechnology) with bovine serum albumin (BSA) as the standard.

Equal amounts of protein (30 μg/lane) were mixed with 5×SDS loading buffer and denatured at 95°C for 10 min. Proteins were separated by 10% (MMP9, NF-κB p65, and Bcl2) or 12% (iNOS, CD38, IL-17A, Cleaved-caspase 3, Bax, and GAPDH) sodium dodecyl sulfate-polyacrylamide gel electrophoresis (SDS-PAGE; Bio-Rad, Hercules, CA, USA) gels at 120 V for 90 min. Separated proteins were transferred onto PVDF membranes (0.45 μm, Bio-Rad) at 300 mA for 90–120 min (4°C), with longer transfer times for high-molecular-weight proteins (iNOS: 131 kDa and IL-17RA: 125 kDa).

Membranes were blocked using 5% non-fat milk (Solarbio, Beijing, China) in TBST, with an incubation duration of 1 h under room temperature conditions. The membranes were incubated overnight at 4°C with primary antibodies (Abcam, Cambridge, UK) at optimized dilutions: anti-iNOS (ab178945, 1:1000, Abcam), anti-CD38 (ab108403, 1:1000, Abcam), anti-MMP9 (ab137867, 1:1500, Abcam), anti-IL-17RA (ab263908, 1:1000, Abcam), anti-NF-κB p65 (ab32536, 1:1000, Abcam), anti-p-NF-κB p65 (ab239882, 1:1000, Abcam), anti-Cleaved-caspase 3 (ab2302, 1:1000, Abcam), anti-Bax (ab182733, 1:1000, Abcam), anti-Bcl2 (ab32124, 1:1000, Abcam), and anti-GAPDH (loading control; ab181602, 1:5000, Abcam). After three TBST washes (10 min each), membranes were incubated with HRP-conjugated goat anti-rabbit IgG (ab6721, 1:10000, Abcam) for 1 h at room temperature. Protein bands were visualized using an ECL detection kit (Beyotime Biotechnology) and a Tanon 5200 chemiluminescence imaging system. Band intensities were assessed *via* ImageJ, and relative expression of the target protein was derived as the ratio between its intensity and that of GAPDH.

Enzyme-linked immunosorbent assay (ELISA)

Levels of TNF-α, IL-6, and IL-17A in cell culture supernatants were quantified using human ELISA kits (R&D Systems, Minneapolis, MN, USA) following the manufacturer's protocols. Supernatants were collected after 24 h of treatment and centrifuged at 1000×*g* for 10 min to remove debris. Standards (recombinant human TNF-α, IL-6, or IL-17A prepared as serial dilutions) and samples (cell culture supernatants) were loaded onto pre-coated wells and incubated for 2 h at room temperature. After washing, biotin-conjugated detection antibodies against human TNF-α, IL-6, or IL-17A were added and incubated for 1 h, followed by streptavidin-HRP incubation for 20 min. Substrate solution was added, and the reaction was stopped with 2 N H_2SO_4. Absorbance was read at 450 nm, and cytokine concentrations were calculated from standard curves.

Flow cytometry

VSMC apoptosis was analyzed using an Annexin V-FITC/PI Apoptosis Detection Kit (Beyotime Biotechnology). After 24 h of co-culture with the macrophages, VSMCs were harvested, washed with PBS, and resuspended in binding buffer. Cells were stained with Annexin V-FITC and propidium iodide (PI) for 15 min in the dark. Apoptosis was quantified using a BD FACSVerse flow cytometer (BD Biosciences, San Jose, CA, USA), and data were analyzed with FlowJo.

Statistical analysis

All experiments were performed with three independent biological replicates ($n = 3$), and each biological replicate was assayed in three technical triplicates. Data were expressed as mean ± standard deviation (SD), with GraphPad Prism 9.0 used to analyze the results. Differences between two groups were compared using an unpaired two-tailed Student's *t*-test, while one-way analysis of variance (ANOVA) followed by Tukey's post-hoc test was used for comparisons among three or more groups. Statistical significance was defined as * $p < 0.05$, ** $p < 0.01$, and *** $p < 0.001$.

Results

Bioinformatics identification of icariin-targeted genes mediating M1 macrophage polarization in AAA

To dissect the molecular crosstalk underlying AAA, M1 macrophage polarization, and icariin intervention, bioin-

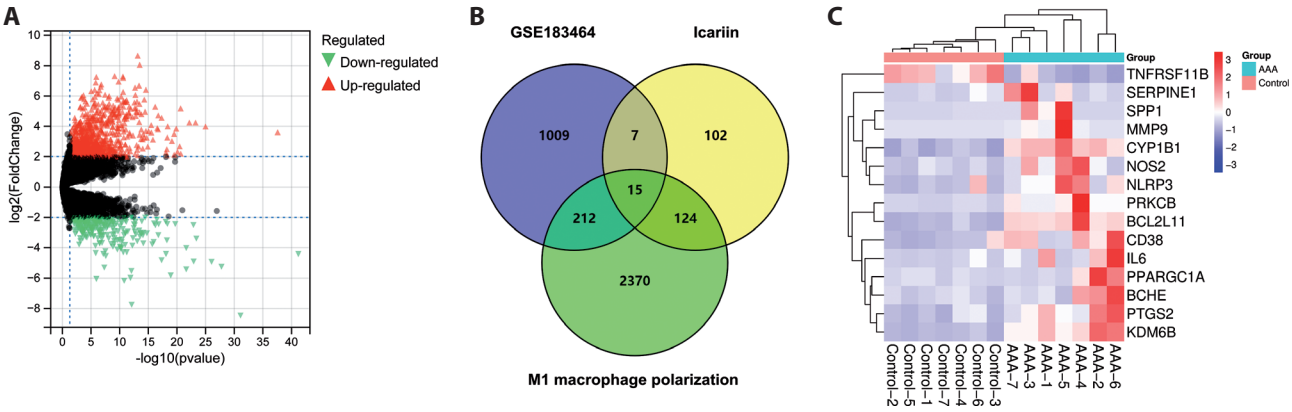

Figure 1. Bioinformatics screening of candidate genes associated with AAA, M1 macrophage polarization, and icariin. **A.** Volcano plot illustrating differential gene expression in AAA *vs.* control tissues from GSE183464 ($p < 0.05$, $|\log_2(\text{fold change})| > 2$); red and green dots denote upregulated and downregulated genes, respectively. **B.** Venn diagram intersecting three gene sets: AAA differential genes, M1 macrophage polarization-related genes, and icariin-targeted genes. **C.** Heatmap showing expression profiles of 15 intersecting genes across 7 AAA and 7 control samples, with hierarchical clustering based on transcriptional patterns.

formatics analyses were performed using the GEO dataset GSE183464. Differential expression profiling revealed extensive transcriptional remodeling in AAA, with 954 upregulated and 289 downregulated genes (Fig. 1A). To identify core candidates at the intersection of these processes, the AAA transcriptional profile was integrated with sets of M1 polarization-related genes and predicted icariin-target genes *via* a Venn analysis (Fig. 1B). This integration yielded 15 candidate genes, implying their potential role in mediating the tripartite interaction. A heatmap of these genes confirmed distinct expression patterns that clearly separated AAA from control samples (Fig. 1C). Notably, genes such as CYP1B1, NOS2, and PRKCB exhibited marked differential expression, reinforcing their candidacy as key regulators.

To further elucidate the biological functions and signaling pathways of these 15 candidate genes in AAA pathogenesis, GO functional enrichment analysis and KEGG pathway enrichment analysis were performed. The results showed that these genes were significantly enriched in BP closely associated with the research focus, including inflammatory response, macrophage activation and polarization, and regulation of vascular smooth muscle cell apoptosis in the GO biological process category (Fig. S1A see in Supplementary material). In the CC category, the genes were enriched in the extracellular region, plasma membrane, and inflammatory factor receptor complex, critical for inflammatory signal transmission and macrophage-VSMC crosstalk (Fig. S1B); in the MF category, enrichment was observed in cytokine binding, NF-κB complex binding, and oxidoreductase activity, key for M1 polarization and inflammatory signal activation (Fig. S1C). KEGG pathway analysis further demonstrated that the 15 candidate genes were predominantly enriched in the NF-κB signaling pathway, TNF signaling pathway, and IL-17 signaling pathway, all of which are pivotal for driving AAA-related chronic inflammation and VSMC apoptosis (Fig. S1D).

Collectively, these analyses identified a core set of 15 genes that bridge AAA pathology, M1 macrophage polarization, and icariin regulation, and further clarified their functional characteristics and key signaling pathways in AAA pathogenesis, laying a foundation for subsequent mechanistic validation.

Machine learning refines core target genes in icariin-mediated AAA pathogenesis

Building on the 15 candidate genes identified earlier, machine learning strategies, namely LASSO regression, and RF, were deployed to prioritize key regulators bridging icariin, M1 macrophage polarization, and AAA. LASSO regression first filtered genes by shrinkage intensity. The coefficient path plot (Fig. 2A) tracked how gene coefficients evolved with increasing log Lambda (λ): as log λ rose, most coefficients diminished toward zero, while five genes (KDM6B, CYP1B1, BCL2L11, CD38, and TNFRSF11B) maintained non-zero values, signifying their robust model relevance. Complementing this, the partial likelihood deviance plot (Fig. 2B) defined the optimal λ (log(λ.min) = −5.4044), striking a balance between model complexity and predictive power to mitigate overfitting.

Following this, the relative importance of the 15 candidates was assessed by RF. The bar plot (Fig. 2C) uncovered PRKCB, CYP1B1, NOS2, and BCL2L11 as top-ranked features, implying their dominant role in distinguishing AAA-associated M1 polarization. To identify genes consistently prioritized by both algorithms, a Venn diagram (Fig.

2D) intersected the gene sets selected *via* LASSO (5 genes) and RF (4 genes). This intersection yielded two overlapping genes: CYP1B1 and BCL2L11.

By integrating the shrinkage-driven selection of LASSO and the feature importance framework of RF, these complementary machine learning approaches converged on these two genes as core candidates, refining the initial set of 15 candidates into a focused set for subsequent mechanistic validation.

Molecular docking validates CYP1B1 as a high-affinity target of icariin

Following the identification of CYP1B1 and BCL2L11 as core candidates *via* machine learning, molecular docking was performed to assess their binding potential with icariin. Molecular docking visualized the 3D interaction profile between icariin and CYP1B1 (Fig. 3A). The global structural view localized icariin within the catalytic cleft of CYP1B1, while the magnified inset uncovered a network of intermolecular interactions: hydrogen bonds (e.g., ASP-492 and ARG-523), van der Waals contacts, and π-alkyl interactions (PRO-160). The calculated binding energy of −8.3 kcal/mol indicated a thermodynamically favorable complex. In contrast, icariin exhibited negligible binding affinity to BCL2L11 (data not shown), eliminating it as a direct molecular target.

To further dissect the interaction landscape, a 2D interaction map (Fig. 3B) delineated residue-specific contacts. Conventional hydrogen bonds (e.g., ARG-523 and ALA-495),

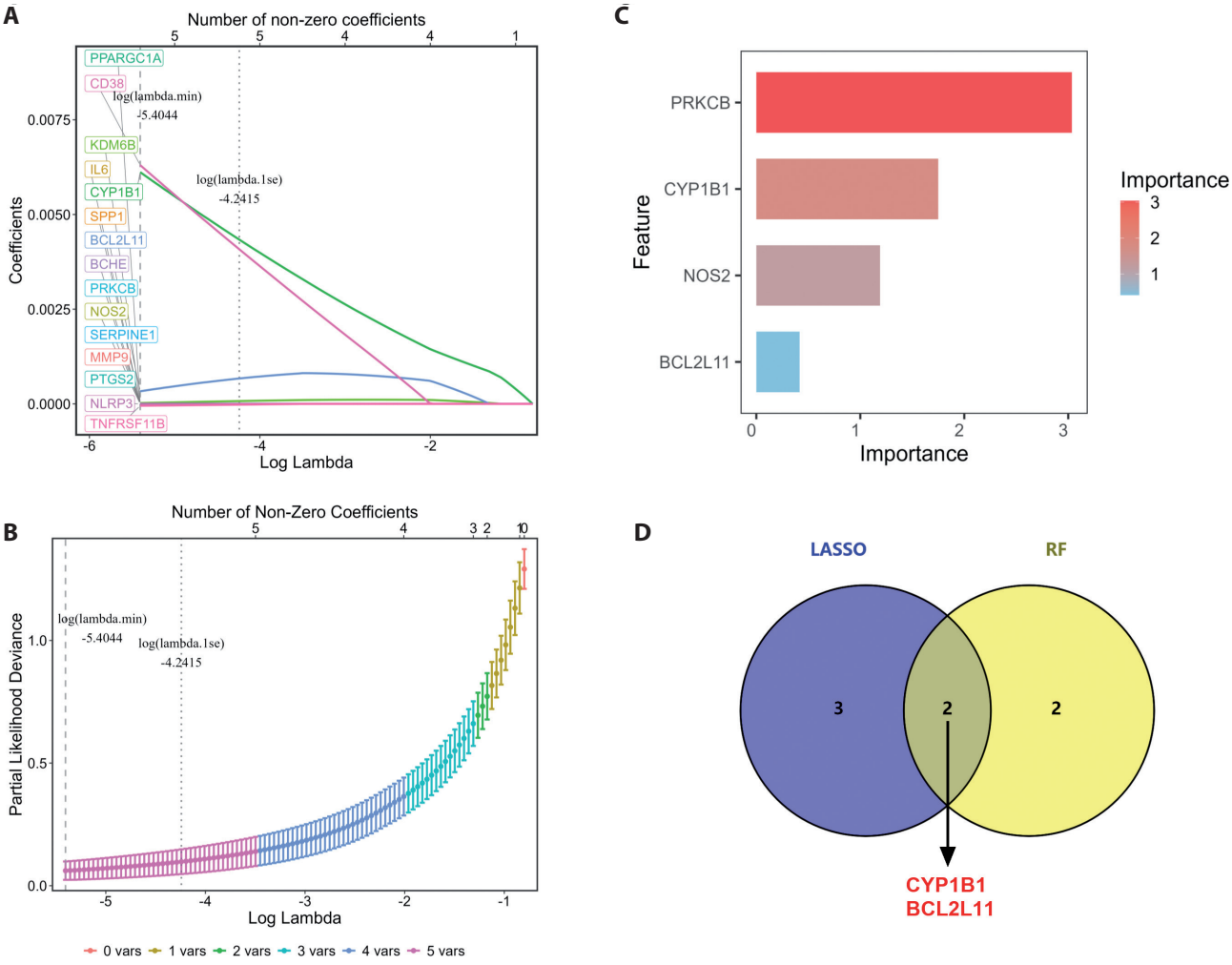

Figure 2. Machine learning-based prioritization of core target genes. **A.** LASSO coefficient path plot depicting coefficient shrinkage across increasing log λ; genes retaining non-zero coefficients at optimal λ are labeled. **B.** Partial likelihood deviance plot for LASSO regression, illustrating the relationship between log λ and model deviance to identify λ.min and λ.1se. **C** RF feature importance plot, where bar height reflects the relative contribution of each candidate gene. **D.** Venn diagram intersecting genes selected by LASSO and RF, highlighting CYP1B1 and BCL2L11 as shared targets.

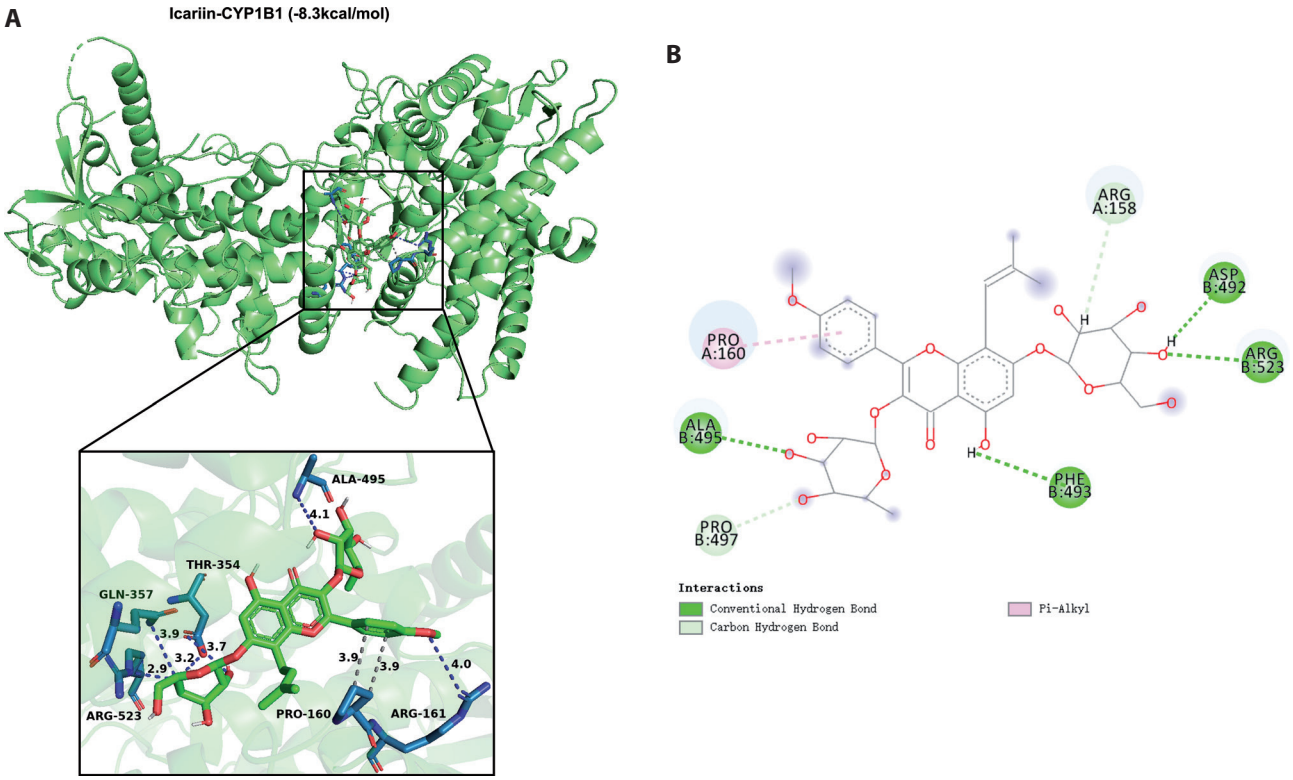

Figure 3. Molecular docking characterization of icariin binding to CYP1B1. **A.** 3D structural model depicting icariin (yellow) docked into the active site of CYP1B1 (gold ribbon), with a magnified view of intermolecular interactions (dashed lines represent hydrogen bonds and π-alkyl contacts). **B.** 2D interaction diagram illustrating specific residue-ligand interactions, color-coded by type: green (conventional hydrogen bonds), pink (π-alkyl interactions), and light green (van der Waals forces). (See online version for color figure.)

carbon-hydrogen bonds, and van der Waals forces synergistically stabilized the icariin-CYP1B1 complex, with key residues (e.g., PRO-160 and GLN-357) forming the critical binding interface.

Cumulatively, these docking analyses confirmed CYP1B1 as a high-affinity target of icariin, providing a structural basis for its potential role in modulating M1 macrophage polarization during AAA pathogenesis.

Icariin suppresses M1 macrophage polarization in THP-1-derived macrophages

Following molecular docking confirmation of icariin's high-affinity binding to CYP1B1, cellular assays were designed to investigate icariin's functional impact on M1 macrophage polarization. To identify a non-toxic concentration range for icariin, cell viability was assessed. The CCK-8 assay demonstrated that concentrations of 5 and 10 μM were well tolerated, while 20 μM and 50 μM significantly impaired cell viability (* $p < 0.05$ and ** $p < 0.01$, respectively; Fig. 4A). Therefore, the non-cytotoxic concentrations of 5 and 10 μM icariin were selected for all subsequent mechanistic studies to ensure that any observed effects were attributable to icariin's specific pharmacological actions rather than general cytotoxicity.

Subsequently, WB (Fig. 4B) analyzed M1 polarization markers (iNOS, CD38, and MMP9). LPS/IFN-γ stimulation markedly upregulated these proteins, whereas icariin co-treatment (5 and 10 μM) dose-dependently attenuated their expression. Quantitative densitometry (Fig. 4C) confirmed robust inhibition: for iNOS, CD38, and MMP9, 10 μM icariin reduced protein levels compared to the LPS/IFN-γ group, indicative of potent suppression of M1 polarization.

Taken together, these findings demonstrated that icariin, at physiologically relevant concentrations, inhibited M1 macrophage polarization in THP-1-derived cells, consistent with its predicted interaction with CYP1B1.

CYP1B1 overexpression reverses icariin-mediated inhibition of M1 polarization and NF-κB signaling

To elucidate whether icariin suppresses M1 macrophage polarization through targeting CYP1B1, gain-of-function experiments were conducted. Robust CYP1B1 overexpres-

sion at the protein level was verified to validate the cellular model for rescue assays (Fig. 5A), which confirmed the model's adequacy for follow-up experiments. Meanwhile, an independent CYP1B1 overexpression group was established to exclude non-specific interference from CYP1B1 overexpression, with no icariin pretreatment or LPS/IFN-γ stimulation. CYP1B1 overexpression alone did not significantly modify the protein levels of M1 polarization markers (iNOS, CD86) or the phosphorylation of NF-κB p65 (Fig. S2). These results confirmed that CYP1B1 overexpression itself exerted no effect on macrophage M1 polarization or NF-κB activity. Building on this, M1 polarization markers (iNOS, CD38, and MMP9) were analyzed *via* WB (Fig. 5B). Icariin-induced suppression of these markers was partially reversed by CYP1B1 overexpression: for iNOS, CD38, and MMP9 protein levels in the CYP1B1-overexpressing group were significantly higher than in the icariin-treated group, indicating CYP1B1-dependent regulation.

To probe the signaling mechanism, the researchers assessed NF-κB activation *via* phosphorylated NF-κB p65 (p-NF-κB p65) (Fig. 5C). LPS/IFN-γ strongly upregulated p-NF-κB p65, which was inhibited by icariin. However, CYP1B1 overexpression restored p-NF-κB p65 levels, suggesting NF-κB as a downstream mediator of CYP1B1 in this pathway. Consistently, ELISA assays (Fig. 5D–F) revealed that icariin reduced LPS/IFN-γ-induced secretion of pro-inflammatory cytokines (TNF-α, IL-17A, and IL-6), while CYP1B1 overexpression partially reversed these effects. This cytokine profile mirrored the M1 polarization phenotype, further supporting CYP1B1's role in mediating icariin's anti-inflammatory actions.

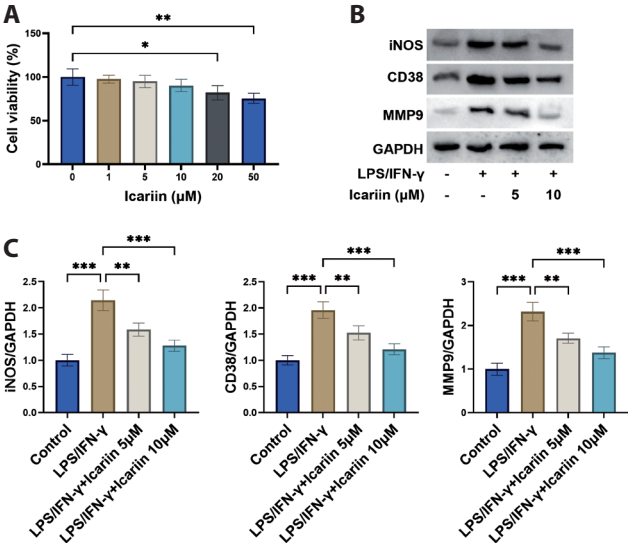

Figure 4. Icariin attenuates M1 macrophage polarization in THP-1-derived macrophages. **A.** CCK-8 assay measuring cell viability in THP-1-derived macrophages treated with icariin (1–50 μM) for 24 h, following differentiation with 100 nM PMA and stimulation with LPS/IFN-γ. **B.** WB detection of M1 polarization markers (iNOS, CD38, and MMP9) in cells grouped as: control, LPS/IFN-γ alone, or LPS/IFN-γ plus icariin (5 and 10 μM). GAPDH was used as a loading control. **C.** Quantitative analysis of protein band intensities normalized to GAPDH, with statistical significance relative to the LPS/IFN-γ group indicated (* $p < 0.05$, ** $p < 0.01$, *** $p < 0.001$).

Thus, these rescue experiments demonstrated that CYP1B1 overexpression counteracted icariin's inhibition of M1 polarization, NF-κB activation, and proinflammatory cytokine production, confirming CYP1B1 as a critical target through which icariin regulates AAA-associated M1 macrophage polarization.

Icariin attenuates vascular smooth muscle cell apoptosis induced by M1 macrophages via CYP1B1 inhibition

Given the pivotal role of VSMC apoptosis in AAA pathogenesis, the study next investigated whether icariin-modulated M1 macrophages influence VSMC survival, focusing on CYP1B1-mediated effects. VSMC apoptosis was evaluated *via* flow cytometry (Fig. 6A) and WB for apoptosis-related proteins (Fig. 6B). Flow cytometry revealed that LPS/IFN-γ-polarized M1 macrophages significantly increased VSMC apoptosis. LPS/IFN-γ + Icariin treatment markedly reduced this apoptosis, whereas CYP1B1 overexpression partially reversed icariin's protective effect. Consistently, results from WB revealed that LPS/IFN-γ induced pro-apoptotic markers (Cleaved-caspase 3 and Bax) and suppressed anti-apoptotic Bcl2. LPS/IFN-γ + Icariin treatment reversed these changes, while CYP1B1 overexpression blunted icariin's effects: Cleaved-caspase 3 and Bax levels increased, and Bcl2 levels decreased compared to the LPS/IFN-γ + Icariin group.

Overall, these results demonstrated that icariin exerted its effects in M1 macrophages in a CYP1B1-dependent manner, thereby mitigating VSMC apoptosis triggered by the pro-inflammatory milieu and revealing a novel protective mechanism against AAA progression.

Discussion

AAA pathogenesis is closely associated with M1 macrophage-driven inflammation and VSMC apoptosis, but the molecular targets mediating these processes remain incompletely defined (Lai et al. 2020). Although natural products have emerged as promising therapeutic agents for cardiovascular diseases, their precise targets often require systematic screening (Sofiullah et al. 2023; Yan et al. 2024). To address this gap, the study employed a multi-step strategy combining bioinformatics, machine learning, and experimental validation.

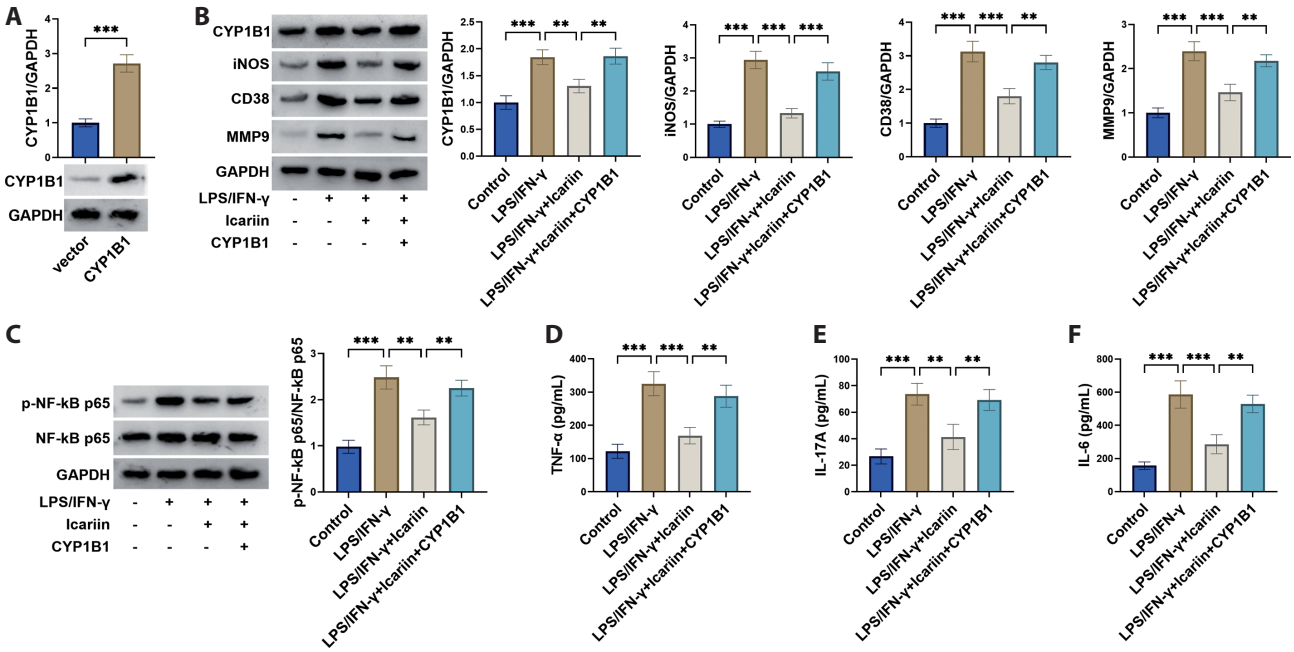

Figure 5. CYP1B1 overexpression abrogates icariin's anti-M1 effects in THP-1-derived macrophages. THP-1-derived macrophages were treated as follows: Control, LPS/IFN-γ, LPS/IFN-γ+Icariin, and LPS/IFN-γ+Icariin+CYP1B1. **A.** WB of CYP1B1 overexpression efficiency. **B.** WB (left) and densitometric analysis (right) of M1 markers (iNOS, CD38, and MMP9). **C.** WB (left) and densitometric analysis (right) of p-NF-κB p65 and total NF-κB p65. ELISA quantification of TNF-α (**D**), IL-17A (**E**), and IL-6 (**F**) in culture supernatants. Statistical significance: ** $p < 0.01$, *** $p < 0.001$ *vs.* indicated groups.

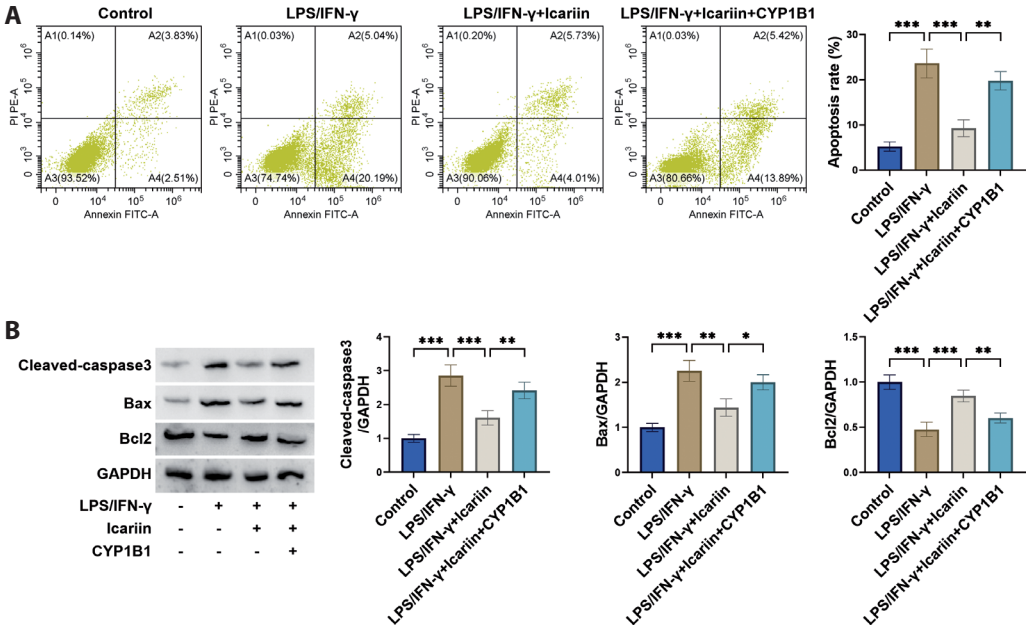

Figure 6. Icariin suppresses VSMC apoptosis induced by M1 macrophages through CYP1B1 inhibition. VSMCs co-cultured with macrophages were divided into four groups as follows: Control, LPS/IFN-γ, LPS/IFN-γ+Icariin, and LPS/IFN-γ+Icariin+CYP1B1. **A.** Flow cytometry plot (Annexin V-FITC/PI staining) and quantification of apoptosis rates. **B.** WB detection of apoptosis-related proteins (Cleaved-caspase 3, Bax, and Bcl2) and densitometric analysis, with GAPDH as loading controls. Statistical significance: * $p < 0.05$, ** $p < 0.01$, *** $p < 0.001$ *vs.* indicated groups.

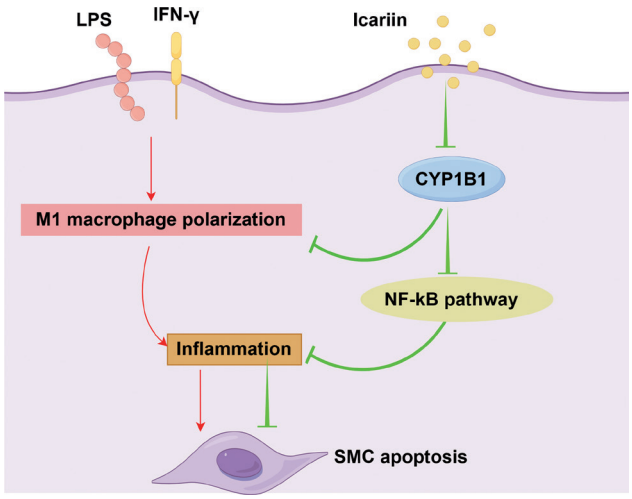

Figure 7. Proposed model of icariin's protective mechanism against AAA.

Following this integrative framework, bioinformatics analysis of the GSE183464 dataset identified 1243 DEGs in AAA tissues, consistent with reports of widespread transcriptional remodeling in AAA (Xiong et al. 2024). Integration with M1 polarization-related and icariin-targeted genes yielded 15 candidates, reflecting the overlapping regulatory networks of inflammation and natural product action (Chen et al. 2025). GO functional enrichment and KEGG pathway analyses of these 15 candidate genes further revealed their significant enrichment in AAA core pathological processes, including M1 macrophage polarization, inflammatory signal activation, and VSMC apoptosis, as well as classic pro-inflammatory signaling pathways such as NF-κB and TNF, which clarified the biological relevance of the candidate genes and provided a solid functional basis for subsequent core target screening. To refine the candidate list, two machine learning techniques were employed: LASSO regression, which is adept at feature selection in high-dimensional data (Liu et al. 2024), and RF, a robust classifier for biological datasets (Nayarisseri et al. 2021). This combined analysis converged on CYP1B1 and BCL2L11 as the top candidates. This dual-algorithm approach enhances target reliability, as demonstrated in previous studies using artificial intelligence to prioritize natural product targets (Zhou et al. 2024).

Subsequently, molecular docking was performed, which revealed icariin bound to CYP1B1 with high affinity *via* hydrogen bonds and π-alkyl interactions, while showing negligible binding to BCL2L11. Molecular docking serves as a widely used structure-based computational strategy in drug discovery and target verification (Muhammed et al. 2024). This selective binding aligns with findings that natural products often interact with CYP450 enzymes to modulate their catalytic activity (Hu et al. 2023; ElKhatib et al. 2024). To functionally validate this interaction, the study confirmed CYP1B1's role in M1 macrophage polarization. Icariin dose-dependently reduced LPS/IFN-γ-induced expression of iNOS, CD38, and MMP9, key M1 markers, while CYP1B1 overexpression reversed these effects. This is consistent with reports that CYP1B1 deficiency impairs macrophage phagocytic function and inflammatory responses (Du et al. 2025) and that CYP1B1 knockdown ameliorated cytokine-induced cellular damage (Teixeira et al. 2022). The study extended these observations by linking CYP1B1 to icariin-mediated anti-inflammatory effects in macrophages.

Having established a role in polarization, the investigation next focused on the underlying signaling pathway. NF-κB is a master regulator of M1 macrophage polarization, and its dysregulation drives AAA progression (Xu et al. 2025). The study found that icariin inhibited LPS/IFN-γ-induced NF-κB p65 phosphorylation, while CYP1B1 overexpression restored NF-κB activation. This aligned with previous work showing CYP1B1 modulated NF-κB activity (Zhu et al. 2025). Consistent with the modulation of NF-κB, proinflammatory cytokine secretion (TNF-α, IL-17A, and IL-6) mirrored NF-κB activation patterns, confirming downstream functional consequences. Similar findings have been reported for other natural products, which suppress macrophage cytokine production *via* NF-κB inhibition (Xu et al. 2022), but the study uniquely tied this pathway to CYP1B1 targeting by icariin.

Given the critical impact of M1 macrophages on vascular integrity, the functional consequence on VSMC apoptosis was then examined. VSMC apoptosis is a hallmark of AAA, driven in part by proinflammatory M1 macrophages (Shioi and Ikari 2018). Inflammatory response, oxidative stress, and abnormal cell death are conserved pathological mechanisms underlying multiple cardiovascular disorders (Singh et al. 2023). The co-culture experiments demonstrated that icariin-treated M1 macrophages reduced VSMC apoptosis, as evidenced by decreased Cleaved-caspase 3/Bax and increased Bcl2 expression – effects reversed by CYP1B1 overexpression. This is consistent with reports that targeting macrophage polarization protects VSMCs in vascular diseases (Pan et al. 2022), and extends these findings by identifying the icariin-CYP1B1 axis as a novel regulatory mechanism. Notably, CYP1B1 has been linked to cellular hypertrophy and fibrosis in other organs (Pingili et al. 2020), but its role in AAA-related VSMC apoptosis is unreported. This suggests that CYP1B1 may act as a conserved regulator of the crosstalk between M1 macrophages and vascular smooth muscle cells across vascular pathologies.

Several limitations of the present study should be stated. First, all mechanistic investigations were performed using *in vitro* cell models, which fail to fully recapitulate the complex inflammatory microenvironment, multicellular crosstalk, and systemic regulatory network of human abdominal aortic

aneurysm *in vivo*. Second, the current study lacks validation from *in vivo* animal models of AAA, which restricts the translational potential of the present findings. Third, the *in vivo* pharmacokinetic properties of icariin, including its absorption, distribution, metabolism, and excretion, have not been explored. Unclear pharmacokinetic characteristics hinder the determination of an optimal administration regimen, which is essential for the further clinical application and translation of icariin. These limitations will be systematically addressed in future research to promote the clinical transformation of icariin.

In conclusion, the study identifies CYP1B1 as a high-affinity target of icariin and demonstrates that icariin inhibits M1 macrophage polarization and subsequent VSMC apoptosis *via* CYP1B1-mediated NF-κB suppression. This work integrates transcriptomic-driven omics screening with experimental validation to unravel a novel regulatory pathway in AAA pathogenesis, while providing an actionable target for AAA therapy, as summarized in the proposed model of Figure 7. The findings support further investigation of icariin and CYP1B1 modulators as potential therapeutic agents for AAA.

Data availability statement. The datasets used and analysed during the current study are available from the corresponding author on reasonable request.

Conflicts of interest. The authors have no interests to disclose.

Authors' contributions. XL conceived and designed the study, and drafted the first draft of the manuscript. All experiments were completed by all authors. SL, JW, ZT analyzed and collated the results. All authors reviewed and critiqued the manuscript, and agreed to the final submission of the manuscript. All authors read and approved the final manuscript.

References

Ahuja A, Murti Y, Singh S (2024): Exploring the potential of artificial intelligence in medical research: applications, regulatory concerns, opportunities and future outlook-a mini review. Lett Drug Des Discov **21,** 4205-4220 https://doi.org/10.2174/0115701808342987241216081153

Chang Z, Zhao G, Zhao Y, Lu H, Xiong W, Liang W, Sun J, Wang H, Zhu T, Rom O (2020): BAF60a deficiency in vascular smooth muscle cells prevents abdominal aortic aneurysm by reducing inflammation and extracellular matrix degradation. Arterioscler Thromb Vasc Biol **40,** 2494-2507 https://doi.org/10.1161/ATVBAHA.120.314955

Chen Y, Wang G, Jiang Y, Qian K, Liu Y, Qiu C, Huang P (2025): Traditional medicine Kuanxiong Aerosol alleviates atherosclerotic plaque inflammation by mitigating CX3CR1+ macrophage apoptosis via the cGAS-STING pathway. Phytomedicine **146,** 157120 https://doi.org/10.1016/j.phymed.2025.157120

Cho MJ, Lee M-R, Park J-G (2023): Aortic aneurysms: current pathogenesis and therapeutic targets. Exp Mol Med **55,** 2519-2530 https://doi.org/10.1038/s12276-023-01130-w

Du Q, Liu K, Li Y, Wang X, Liu X, Zhao J, Wang X (2025): Inhibition of CYP450 family 1 subfamily B member 1 (CYP1B1) expression in macrophage reduces the inflammatory response in type 2 diabetes mellitus combined with tuberculosis. Front Endocrinol (Lausanne) **16,** 1617292 https://doi.org/10.3389/fendo.2025.1617292

ElKhatib MA, Gerges SH, Isse FA, El-Kadi AO (2024): Cytochrome P450 1B1 is critical in the development of TNF-α, IL-6, and LPS-induced cellular hypertrophy. Can J Physiol Pharmacol **102,** 408-421 https://doi.org/10.1139/cjpp-2024-0037

Fang J, Zhang Y (2017): Icariin, an anti-atherosclerotic drug from Chinese medicinal herb horny goat weed. Front Pharmacol **8,** 734 https://doi.org/10.3389/fphar.2017.00734

Haque K, Bhargava P (2022): Abdominal aortic aneurysm. Am Fam Physician **106,** 165-172

Hu B, Zhao X, Wang E, Zhou J, Li J, Chen J, Du G (2023): Efficient heterologous expression of cytochrome P450 enzymes in microorganisms for the biosynthesis of natural products. Crit Rev Biotechnol **43,** 227-241 https://doi.org/10.1080/07388551.2022.2029344

Huang R, Sun Y, Liu R, Zhu B, Zhang H, Wu H (2024): ZeXieYin formula alleviates atherosclerosis by inhibiting the MAPK/NF-κB signaling pathway in APOE−/− mice to attenuate vascular inflammation and increase plaque stability. J Ethnopharmacol **327,** 117969 https://doi.org/10.1016/j.jep.2024.117969

Lai C-H, Chang C-W, Lee F-T, Kuo C-H, Hsu J-H, Liu C-P, Wu H-L, Yeh J-L (2020): Targeting vascular smooth muscle cell dysfunction with xanthine derivative KMUP-3 inhibits abdominal aortic aneurysm in mice. Atherosclerosis **297,** 16-24 https://doi.org/10.1016/j.atherosclerosis.2020.01.029

Liu Y, Gao Q, Wei K, Huang C, Wang C, Yu Y, Qin G, Wang T (2024): High-dimensional generalized median adaptive lasso with application to omics data. Brief Bioinform **25,** bbae059 https://doi.org/10.1093/bib/bbae059

Lu H, Du W, Ren L, Hamblin MH, Becker RC, Chen YE, Fan Y (2021) Vascular smooth muscle cells in aortic aneurysm: from genetics to mechanisms. J Am Heart Assoc **10,** e023601 https://doi.org/10.1161/JAHA.121.023601

Muhammed MT, Aki-Yalcin E (2024): Molecular docking: principles, advances, and its applications in drug discovery. Lett Drug Des Discov **21,** 480-495 https://doi.org/10.2174/1570180819666220922103109

Nayarisseri A, Khandelwal R, Tanwar P, Madhavi M, Sharma D, Thakur G, Speck-Planche A, Singh SK (2021): Artificial intelligence, big data and machine learning approaches in precision medicine & drug discovery. Curr Drug Targets **22,** 631-655 https://doi.org/10.2174/18735592MTEzsMDMnz

Ogbonna UE, Ofoezie EF, Babalola OO, Ottu PO, Ogbonna CA, Olisakwe S, George TE, Babarinde S, Omaba JO, Chukwuemeka CG, Amafili CC, Afamefuna A, Ogbonna H (2025): Advances in machine learning for optimizing pharmaceutical drug discovery. Current Proteomics **22,** 100015

https://doi.org/10.1016/j.curpro.2025.100015
Pan L, Bai P, Weng X, Liu J, Chen Y, Chen S, Ma X, Hu K, Sun A, Ge J (2022) Legumain is an endogenous modulator of integrin αvβ3 triggering vascular degeneration, dissection, and rupture. Circulation **145,** 659-674
https://doi.org/10.1161/CIRCULATIONAHA.121.056640
Pingili AK, Jennings BL, Mukherjee K, Akroush W, Gonzalez FJ, Malik KU (2020) 6β-Hydroxytestosterone, a metabolite of testosterone generated by CYP1B1, contributes to vascular changes in angiotensin II-induced hypertension in male mice. Biol Sex Differ **11,** 4
https://doi.org/10.1186/s13293-019-0280-4
Puertas-Umbert L, Almendra-Pegueros R, Jimenez-Altayo F, Sirvent M, Galán M, Martínez-González J, Rodríguez C (2023): Novel pharmacological approaches in abdominal aortic aneurysm. Clinical Science **137,** 1167-1194
https://doi.org/10.1042/CS20220795
Sánchez-Gutiérrez M, Izquierdo-Vega AJ, Madrigal-Santillán EO, Velázquez-González C, Izquierdo-Vega JA (2024): Icariin as a treatment proposal in mammalian reproduction. Pharmaceuticals **17,** 1104
https://doi.org/10.3390/ph17091104
Shioi A, Ikari Y (2018): Plaque calcification during atherosclerosis progression and regression. J Atheroscler Thromb **25,** 294-303
https://doi.org/10.5551/jat.RV17020
Singh K, A. Alameri A, Ali Hamza A, E. Al-Gazally M, Temurovich Islomov S, Fadhel Obaid R, Alexis Ramirez-Coronel A, Abosaooda M, Yahyapour R, Najafi M (2023): Cardiac injury following chemo/radiation therapy: an updated review on mechanisms and therapeutic approaches. Curr Radiopharm **16,** 185-203
https://doi.org/10.2174/1874471016666230214101830
Sofiullah SSM, Murugan DD, Muid SA, Seng WY, Kadir SZSA, Abas R, Ridzuan NRA, Zamakshshari NH, Woon CK (2023) Natural bioactive compounds targeting NADPH oxidase pathway in cardiovascular diseases. Molecules **28,** 1047
https://doi.org/10.3390/molecules28031047
Teixeira LD, Harrison NA, da Silva DR, Mathews CE, Gonzalez CF, Lorca GL (2022): Nanovesicles from Lactobacillus johnsonii N6. 2 reduce apoptosis in human beta cells by promoting AHR translocation and IL10 secretion. Front Immunol **13,** 899413
https://doi.org/10.3389/fimmu.2022.899413
Wang Q, Chen G, Qi Z, Zeng Y, Tan L, Tang H (2023): Global research status analysis of the association between aortic aneurysm and inflammation: a bibliometric analysis from 1999 to 2023. Front Cardiovasc Med **10,** 1260935
https://doi.org/10.3389/fcvm.2023.1260935
Xiong J, Chen G, Lin B, Zhong L, Jiang X, Lu H (2024): Integrative analysis of single-Cell RNA sequencing and experimental validation in the study of abdominal aortic aneurysm progression. Gene **929,** 148820
https://doi.org/10.1016/j.gene.2024.148820
Xu R, Ma L, Chen T, Wang J (2022): Sophorolipid suppresses LPS-induced inflammation in RAW264. 7 cells through the NF-κB signaling pathway. Molecules **27,** 5037
https://doi.org/10.3390/molecules27155037
Xu S, Han X, Yu Y, Qu C, Yang B, Shen B, Liu X (2025): Deficiency of IL-7R attenuates abdominal aortic aneurysms in mice by inhibiting macrophage polarization towards M1 phenotype through the NF-κB pathway. Mol Med **31,** 138
https://doi.org/10.1186/s10020-025-01209-2
Yan Q, Song C, Liu H, Li Y, Ma J, Zhao Y, Song Z, Chen Y, Zhu R, Zhang Z (2024): Adipose-derived stem cell exosomes loaded with icariin attenuated M1 polarization of macrophages via inhibiting the TLR4/Myd88/NF-κB signaling pathway. Int Immunopharmacol **137,** 112448
https://doi.org/10.1016/j.intimp.2024.112448
Zhou G, Lin Z, Miao Q, Lin L, Wang S, Lu K, Zhang Y, Chu Q, Kong W, Wu K (2024): Mechanisms of QingRe HuoXue formula in atherosclerosis treatment: An integrated approach using bioinformatics, machine learning, and experimental validation. Int Immunopharmacol **141,** 112890
https://doi.org/10.1016/j.intimp.2024.112890
Zhu S, Cheng L, Chen T, Liu X, Zhang C, Aji A, Guo W, Zhu J, Chu Y, Guo D (2025): Bergapten ameliorates psoriatic skin lesions and IL-17A-induced activation of the NF-κB signaling pathway via the downregulation of CYP1B1. Phytotherapy Research **39,** 661-675
https://doi.org/10.1002/ptr.8399

Received: November 18, 2025
Final version accepted: March 17, 2026